2024 IEEE Applied Power Electronics Conference and Exposition (APEC)

An Asymmetric Perturbation Signal for Enhanced Perturbation Injection Capabilities of a Grid-connected Converter

J. Mace, A. Cervone, and D. Dujic

POWER ELECTRONICS LABORATORY
ÉCOLE POLYTECHNIQUE FÉDÉRALE DE LAUSANNE

An Asymmetric Perturbation Signal for Enhanced Perturbation Injection Capabilities of a Grid-connected Converter

Jules Mace, Andrea Cervone, Drazen Dujic
Power Electronics Laboratory - PEL
École Polytechnique Fédérale de Lausanne - EPFL
Lausanne CH-1015, Switzerland
jules.mace@epfl.ch, andrea.cervone@epfl.ch, drazen.dujic@epfl.ch

***Abstract*—Impedance estimation is an important tool for grid-converter interaction evaluation. Using existing grid-connected converters for perturbation injection enables grid impedance estimation during operation without additional hardware (namely dedicated perturbation injection equipment). However, such equipment (e.g. converters for PV systems, BESS, EV charging stations...) have limited voltage reserve, leading to reduced perturbation injection capabilities (i.e. perturbation magnitude) with conventional perturbation signals (pseudo-random binary signals or chirp signals). To enhance the perturbation capabilities of those converters, an asymmetric signal is proposed that increases the perturbation magnitude at a maximum operating point. An extension to a wide-bandwidth chirp signal is then presented.**

I. Introduction

With the increase of converter-based systems (distributed energy resources, HVDC links, battery energy system storage), grid stability is an important concern for grid operators as some instability events [1], [2], [3] have occurred, caused by an interaction between installed converters and the grid. These events are caused by the connection of unmatching grid impedance and converter output admittance. Therefore, impedance estimation is an important research topic in the power electronics community as it allows grid monitoring (with an impedance estimation done during grid operation) [4], [5], [6], grid event detection (e.g. grid reconfigurations) [7], [8] and potentially converter adaptation [9], [10] during grid operation.

Perturbation injection converters are conventional perturbation injection devices that are used for grid impedance (or converter admittance) estimation. Compared to other methods (passive and active non-invasive techniques [11], [12]), they allow refined shaping of the perturbation injected, for desired injection time, magnitude (small-signal or large-signal) and frequency content (single tone or wide-bandwidth signals). During grid operation, it can be interesting to estimate the grid impedance for grid condition monitoring [3] or converter controller peak adaptation [8], [9]. A perturbation injection can be achieved as in Fig. 1a, however utilizing the existing grid-connected converters as in Fig. 1b is a more interesting solution as it is non-invasive (no additional hardware is installed in the grid) provided that the power hardware and control software of the already grid connected converter are capable of doing so.

However, as they have not been designed for perturbation injection, such converters have many limitations: limited controller bandwidth (addressed in [13]) and limited voltage reserve in their DC links for perturbation injection. The voltage reserve defined in this paper is the difference between the currently applied converter voltage (that depends on the operating point) and the maximum realizable voltage (that depends on the DC-link voltage of the converter). This voltage reserve impacts the maximum perturbation voltage that can be generated by the converter, therefore, during a grid operation where the converter is operating at very large modulation index, the available voltage reserve is limited and its perturbation injection capability is reduced. Naturally, during grid undervoltages, available voltage reserve may actually be sufficient for reliable injection, but this also means that system identification could not be performed at any time and on demand.

Furthermore, most of the conventional perturbation signals for small signal analysis (single tone [3], wide-bandwidth [14], [13]) are symmetric signals, meaning that the positive and negative peaks are centered around zero. A small voltage reserve limits hence not only the positive peak but the total voltage

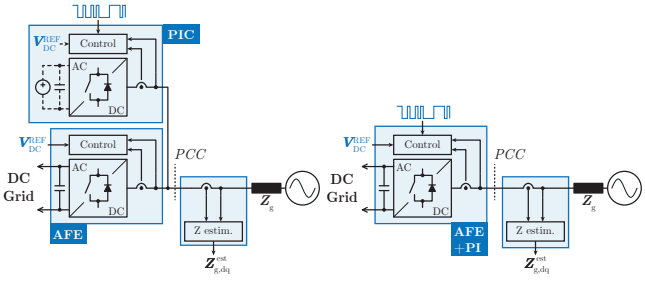

Fig. 1: Grid impedance estimation systems during grid operation at the point of common coupling between an active front end converter (AFE) and an AC grid: (a) a separate perturbation injection converter (PIC) is inserted to generate perturbations, (b) the AFE performs perturbation injection on top its function (e.g. power or voltage regulation for instance).

979-8-3503-1664-3/24/$31.00 ©2024 IEEE

magnitude, affecting directly the quality of the impedance estimation. In this paper, an asymmetric signal is proposed to increase the magnitude of the perturbation in case of limited voltage reserve. The potential of asymmetric impulse signals for impedance estimation has been investigated in [15] but no asymmetric continuous perturbation signal has yet been proposed or investigated.

II. Voltage Reserve of Grid-Connected Converters

The voltage reserve is the difference between the applied converter voltage and the maximum realizable converter phase voltage:

$$\boldsymbol{V}_{\text{reserve}} = \boldsymbol{V}_{\text{c,MAX}} - \boldsymbol{V}_{\text{c,O.P.}} \tag{1}$$

The maximum converter phase voltage depends of the DC-link voltage and is equal to $\frac{1}{\sqrt{3}}V_{\text{DC}}$ when zero sequence injection is applied to the modulator. The actual converter voltage on the other hand, depends on many parameters: the converter output filter and grid impedances, the power flowing to (or from) the AC grid and the actual value of the AC grid voltage.

$$\begin{cases} \boldsymbol{V}_{\text{c,MAX}} = \frac{1}{\sqrt{3}}\boldsymbol{V}_{\text{DC}} \\ \boldsymbol{V}_{\text{c,O.P.}} = \boldsymbol{Z}_{\text{filter}} \cdot \boldsymbol{I}_{\text{c}} + \boldsymbol{Z}_{\text{g}} \cdot \boldsymbol{I}_{\text{g}} + \boldsymbol{V}_{\text{grid}} \end{cases} \tag{2}$$

The generated converter voltage hence changes with the operating point, as shown in Fig. 2, where the trajectory of the voltage vectors in different points of a grid-connected converter are plotted for two different operating points, namely *Operating Point 1* (characterized by a smaller operating voltage, and therefore by a higher voltage reseve) and *Operating Point 2* (characterized by a higher operating voltage, and therefore a smaller voltage reserve).

The grid filter is typically designed to attenuate the harmonics. This filtering effect can pose challenges for impedance estimation since perturbations generated at the converter voltage $\boldsymbol{v}_{\text{c}}$ are reduced significantly on the grid side voltage $\boldsymbol{v}_{\text{g}}$ as it can be seen in Fig. 2. The attenuation introduced by the grid filter can impact differently the perturbation injection capabilities of the converter according to its operating conditions. By referring to the examples of Fig. 2, at the *Operating Point 1*, the converter voltage is far away from the limit offering a large voltage reserve for generating a perturbation with a large magnitude. Such perturbation at the grid side (after the filter) would be reduced but it would remain usable for impedance identification purposes, providing that its magnitude is higher than the noise level of the sensing equipment. However, in the *Operating Point 2*, where the operating voltage is close to the limit, the converter can only generate a perturbation of reduced magnitude. After the attenuation introduced by the grid filter, the remaining voltage perturbation available on the grid side would likely have such a small magnitude to be indistinguishible from the sensor noise, which would make the perturbation not usable for impedance identification. The operating point therefore impacts the maximum generated converter voltage and as a result, in some operating point, the limited magnitude of the injected perturbation might not be enough to produce useful results.

As a consequence, converters with limited DC-link voltage may not offer impedance estimation capability for all operating points. Existing grid connected converters, that are normally designed to work with limited DC-link voltages (i.e., to operate at high modulation index in rated conditions) could only perturb the grid in some specific conditions and times, limiting their applicability for grid impedance estimation.

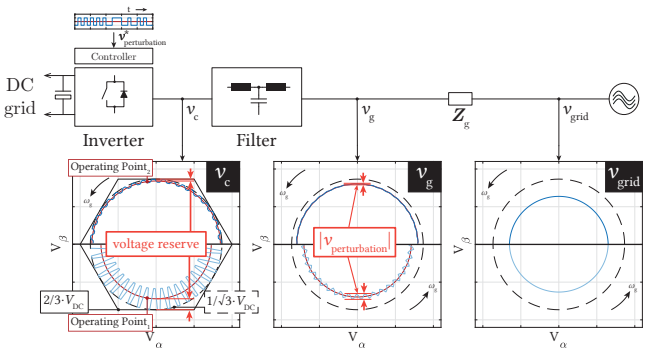

Fig. 2: Perturbation injection for different operating points.

III. Asymmetric signal

The limitations introduced by a reduced voltage reserve can be partially mitigated by employing perturbation injection signals different from the ones typically used in impedance estimation algorithms.

The conventional signals (single tone [3], pseudo-random binary signals (PRBS) [6], chirp signals [14]) used for perturbation injection have the property to be symmetric (as in Fig. 3a), with positive and negative peaks centered around zero.

With a symmetric perturbation signal, the maximum magnitude of the perturbation is limited by the maximum peak voltage that the converter can generate (depending on the DC-bus voltage). However, using an asymmetric signal (with positive and negative peaks not centered around zero), can allow increasing the magnitude of the perturbation harmonics without trespassing the maximum peak voltage constraint.

An example of such signal is given in Fig. 3b. The signal is a square wave with different positive and negative peaks and it is centered around zero thanks to a duty cycle δ that varies with the peak ratio K^-/K^+, defined as follows:

$$\delta = \frac{K^-}{K^+ + K^-} \tag{3}$$

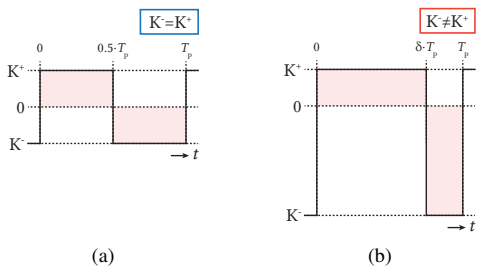

Fig. 3: Shape of (a) a symmetric signal and (b) an asymmetric signal

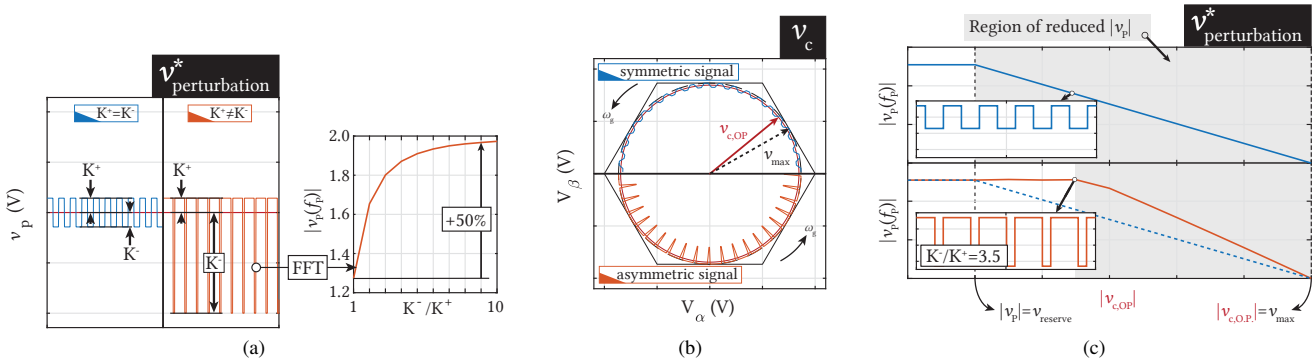

(a) (b) (c)

Fig. 4: (a) symmetric and asymmetric voltages, (b) resulting converter voltages, (c) perturbation voltage magnitudes for different operating points.

It allows for up to 50 % magnitude increase at the perturbation frequency, whilst not saturating the converter voltage (Figs. 4a and 4b). This can therefore enable larger perturbation signal magnitudes beyond the voltage reserve (when $v_P > v_{reserve}$) as shown in Fig. 4c.

A. *Wide-bandwidth perturbation*

To go even further, conventional perturbation signals employed for impedance injection are wide-band signals (PRBS, chirp signals) and with a very simple adaptation of the signal generator (Fig. 5a to Fig. 5b), it is possible to generate asymmetric square chirp signals. This asymmetry causes the signal frequency content (as plotted in Fig. 5d) to be heavily distorted but also, for some frequencies, to go to much higher magnitudes. This second property is very beneficial for impedance estimation as, at those frequency points with larger magnitudes, the signal to noise ratio is increased, leading to much more accurate impedance estimation. The relationship between peak ratio and signal magnitude can also be well expressed in Fig. 6a, where, as the ratio increases, the magnitude of the perturbation frequency band also increases, along with the magnitude of all the harmonic bands ($[k \cdot f_{chirp,beg}, k \cdot f_{chirp,end}]$).

The results presented of Fig. 5 and Fig. 6a are considering narrow-band signals, with a very small perturbation frequency band. Fig. 6b illustrates what happens to the frequency content as the band is enlarged. As the frequency band widens, the harmonic frequency bands widen to eventually merge together, altering the uniform shape of the frequency band. Magnitudes are also reduced, yet they remain comparatively much larger than with a sinusoidal chirp signal. By looking at the frequency distribution of one sine sweep and two square sweeps in Fig. 7, we can see that the spectrum is both shifted to higher magnitudes and much noisier when the square sweep is employed, compared to when the sine sweep is employed. This means that, when the proposed asymmetric signal is used for wide band perturbation, the aliasing between the harmonic bands is such that, in the resulting spectrum, the magnitude of some harmonic beams is enhanced, while is some other beams is reduced. Nonetheless, compared to standard symmetric injection signals, the proposed solution keeps, on average, a higher perturbation injection magnitude, which is beneficial for impedance estimation purposes.

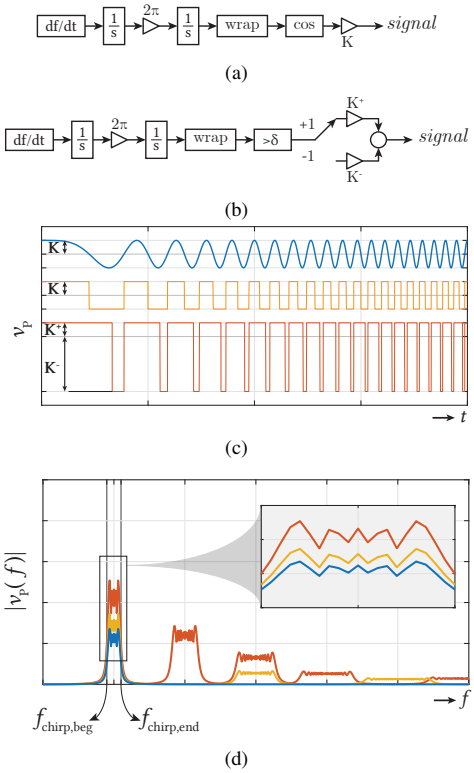

Fig. 5: (a) conventional square chirp signal generator, (b) asymmetric square chirp signal generator, (c) signal shape, (d) frequency decomposition

To express the curve of Fig. 7a in a more comprehensive way, the density of the frequency beans over the full magnitude range has been drawn in Fig. 7b. The density is defined as the proportion of frequency beans in a given magnitude range. In case of the sine chirp signal, the density is very high around the median value, meaning that the frequency beans are very concentrated around the median value. On the other hand, the two square chirp signals have a flatter density curve with a median value located at a higher magnitude value. This means that the beans are more spread (this can also be well seen in the frequency distribution) but have on average a higher magnitude.

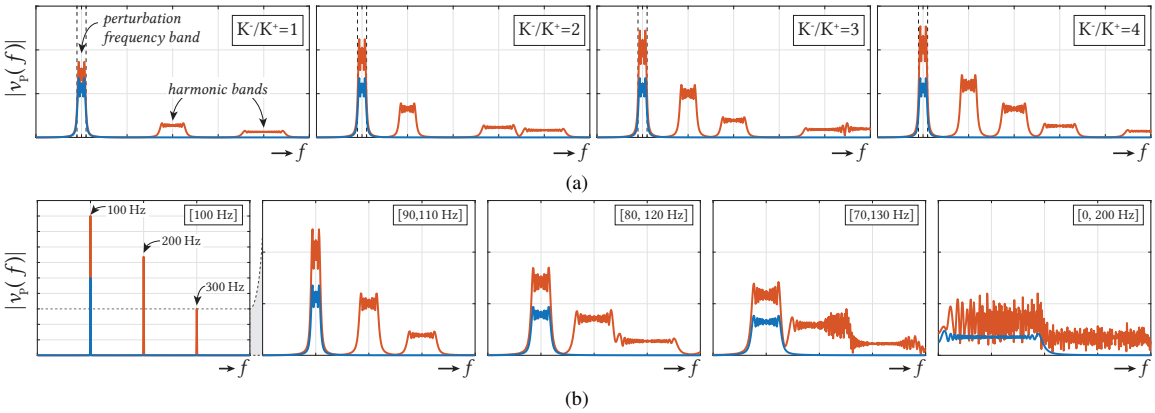

Fig. 6: Frequency content of (a) asymmetric chirp signals with different peak ratios and (b) asymmetric chirp signals with different frequency bands.

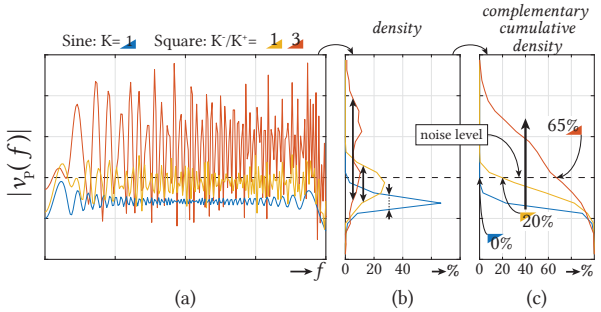

Fig. 7: (a) Wide-bandwidth sinesweep for symmetric sine chirp and square asymmetric chirp signals with distribution of frequency beans over the voltage magnitude interval (b) frequency beans density (c) complementary cumulative density.

Another metric can help illustrating the potential of wide-bandwidth square sweep signals. The complementary cumulative density represents the proportion of points above a given magnitude and it is drawn for the three specific signals in Fig. 7c. Considering injecting a small perturbation in a noisy environment with a noise level below which, the voltages cannot be measured accurately. With the noise level drawn in Fig. 7, no frequency bean of the sine sweep is above it leading to a complementary cumulative distribution of 0%. In the case of a square sweep however, its complementary cumulative distribution is 20% for the peak ratio of 1 and 65% for the peak ratio of 3. This is equivalent of saying that 20% of the frequency beans are above the noise level (for the signal with a peak ratio of 1), also meaning that 20% of the signal would then be usable. This complementary cumulative distribution is hence giving a good indication of the overall magnitude and hence applicability of a perturbation signal and it also shows the superiority of a square signal over a sine signal.

IV. Experimental Results

A. Experimental Setup and Estimation Procedure

An experimental setup presented in Fig. 8 is employed to evaluate the usability of the proposed signal for the impedance estimation. The active front end converter (AFE) is a low voltage medium power converter (45 kVA-rated) with an inverter and filter whose ratings are given in Table I. The AFE is controlling the DC bus voltage and the reactive power injected

Table I: Active Front End Converter Ratings

Parameter	Value
S	45 kVA
V_{DC}	600 V to 800 V
f_{sw}	8 kHz
f_{bw}	1 kHz
L_c	600 µH
C	100 µF
L_g	300 µH

in the AC grid. On top of these functions, it is sending perturbations to the grid by adding to the d- and q-axes converter reference voltages successively the desired perturbation signal [14]. The signal will either be the conventional symmetric sine chirp signal or the asymmetric square chirp signal. The grid voltages and currents are then captured by the data acquisition device and the impedance is finally computed on PC. The estimated impedances will be compared when the sine and square chirp signals are employed. The grid impedance is emulated by a grid emulator (Regatron TC.ACS controlled by a Plexim RT Box).

The impedance is estimated in the dq reference frame following the methods developed by [6], [16], [14], [8], [9]. Two perturbations are injected on the d and then q axes consecutively and the recorded grid and currents are then post-processed using the procedure described in Fig. 9. Firstly, the grid angle is estimated using a conventional phase-locked loop (PLL) [16], [17]. After the grid voltages and currents are transformed in the dq reference frame, frequency components are extracted using an FFT. Finally, the impedance is estimated using the conventional formula [18] to reduce the uncorrelated noise:

$$\boldsymbol{Z}_{\mathrm{g,dq}} = \begin{bmatrix} Z_{\mathrm{g,dd}} & Z_{\mathrm{g,qd}} \\ Z_{\mathrm{g,dq}} & Z_{\mathrm{g,qq}} \end{bmatrix} = \boldsymbol{V}_{\mathrm{g,dq}} \cdot \boldsymbol{I}_{\mathrm{g,dq}}^{-1} \tag{4}$$

where

$$\boldsymbol{V}_{\mathrm{g,dq}}(f) = \begin{bmatrix} v_{\mathrm{g,d}}^{1} & v_{\mathrm{g,d}}^{2} \\ v_{\mathrm{g,q}}^{1} & v_{\mathrm{g,q}}^{2} \end{bmatrix}, \boldsymbol{I}_{\mathrm{g,dq}}(f) = \begin{bmatrix} i_{\mathrm{g,d}}^{1} & i_{\mathrm{g,d}}^{2} \\ i_{\mathrm{g,q}}^{1} & i_{\mathrm{g,q}}^{2} \end{bmatrix} \tag{5}$$

where $\boldsymbol{v}_{\mathrm{g,dq}}^{inj}/\boldsymbol{i}_{\mathrm{g,dq}}^{inj}$ are the voltages and currents of the first or second injection ($inj = 1$ or 2 respectively). The perturbation injection signals being the main focus of this research, only

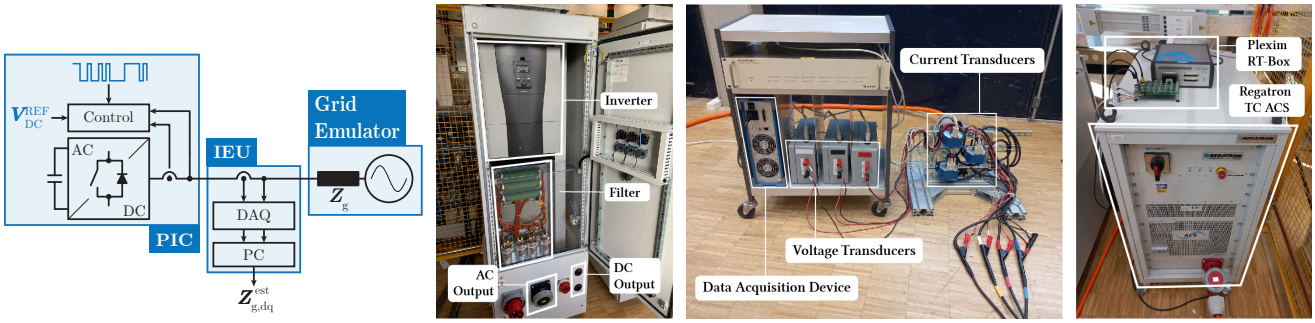

(a) (b) (c) (d)

Fig. 8: Impedance measurement setup (a) scheme with (b) the perturbation injection converter (PIC) injecting currents perturbations into the grid, (c) an Impedance Estimation Unit (IEU) measuring and recording the currents and voltages and computing the estimated impedance and (d) the grid emulator (Regatron TC ACS) emulating a grid with a given $\boldsymbol{Z}_g$.

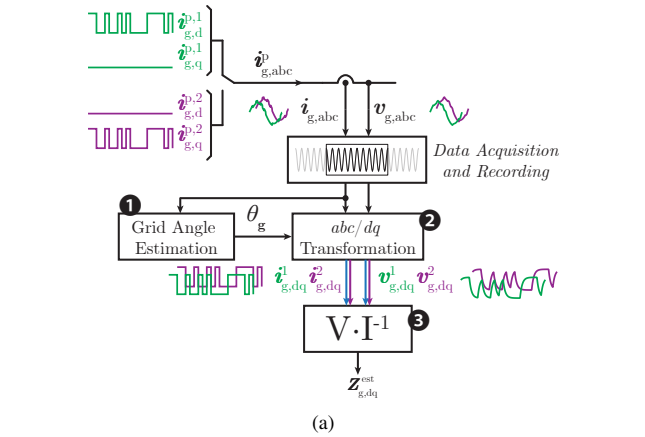

(a) (b) (c) (d)

Fig. 9: Impedance measurement procedure: (a) full procedure with (b) the grid angle estimator, (c) the detailed procedure for the abc/dq transformation and finally (d) the impedance estimation.

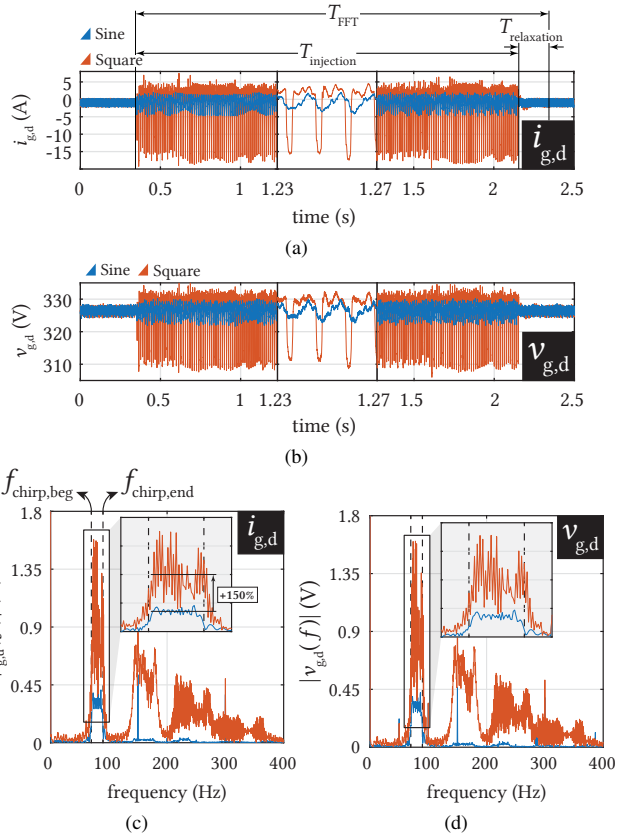

(a) (b) (c) (d)

Fig. 10: Narrow-bandwidth chirp perturbation injection: $[f_{\text{chirp,beg}}, f_{\text{chirp,end}}] = [70\,\text{Hz}, 90\,\text{Hz}]$ ($K^+ = 10\,\text{V}$, $T_{\text{FFT}} = 2\,\text{s}$, $T_{\text{injection}} = 1.9\,\text{s}$, $T_{\text{relaxation}} = 0.1\,\text{s}$), (a) currents and (b) voltages during the perturbation and (c), (d) their respective frequency decomposition.

the grid voltages and currents under perturbation injection are shown in the following section.

B. Narrow-bandwidth perturbation

The converter is connected to a resistive grid (a 400 Vac grid with a purely resistive impedance of 2 Ω, emulated by the grid emulator) and a narrow-bandwidth perturbation is injected in the d axis of the converter voltages. Experimental results are presented in Fig. 10. In this experiment, a symmetric and an asymmetric ($K^-/K^+ = 4$) chirp signals of 10 V magnitude are injected to the converter voltage references. The injection time is 1.9 s and the FFT is performed on a 2 s time interval that includes the injection time and a small relaxation time after the injection. This relaxation time is added to allow the system to settle back to a steady-state operation. As expected from Section III-A and Fig. 5d, the asymmetric signal has a much larger magnitude in the perturbation spectrum $[f_{\text{chirp,beg}}, f_{\text{chirp,end}}]$ (more than 150 % more on average) and it also contains rich energy content outside of this spectrum, following the pattern drawn in Fig. 6. The difference between Fig. 6 and Fig. 10 comes from the measurement after the filter, using a non-ideal converter, with a limited switching frequency.

C. Wide-bandwidth perturbation

Under the same grid conditions, wide-bandwidth perturbation injection is also performed. The frequency sweep is going between 0 Hz and 4 kHz to be close to the switching frequency of the converter. The perturbation time interval is chosen to be 3.9 s, larger than the narrow-bandwidth signal to have higher frequency magnitudes and the peak ratio K^-/K^+ is varied between 1 and 4. Currents and voltages over time and over frequency are plotted in Fig. 11. As seen in both Fig. 11a and Fig. 11c, when the frequency increases, the current magnitude decreases as the converter has a limited bandwidth and this observation is especially true above 1.5 kHz (converter filter resonant frequency).

The current and voltage magnitudes during square chirp perturbations are also much larger than during sine chirp perturbations, even for a peak ratio of 1. As predicted by Section III-A, the peak ratio influences largely the frequency magnitude density. As it increases, the frequency magnitudes increase and spread more over a larger magnitude interval.

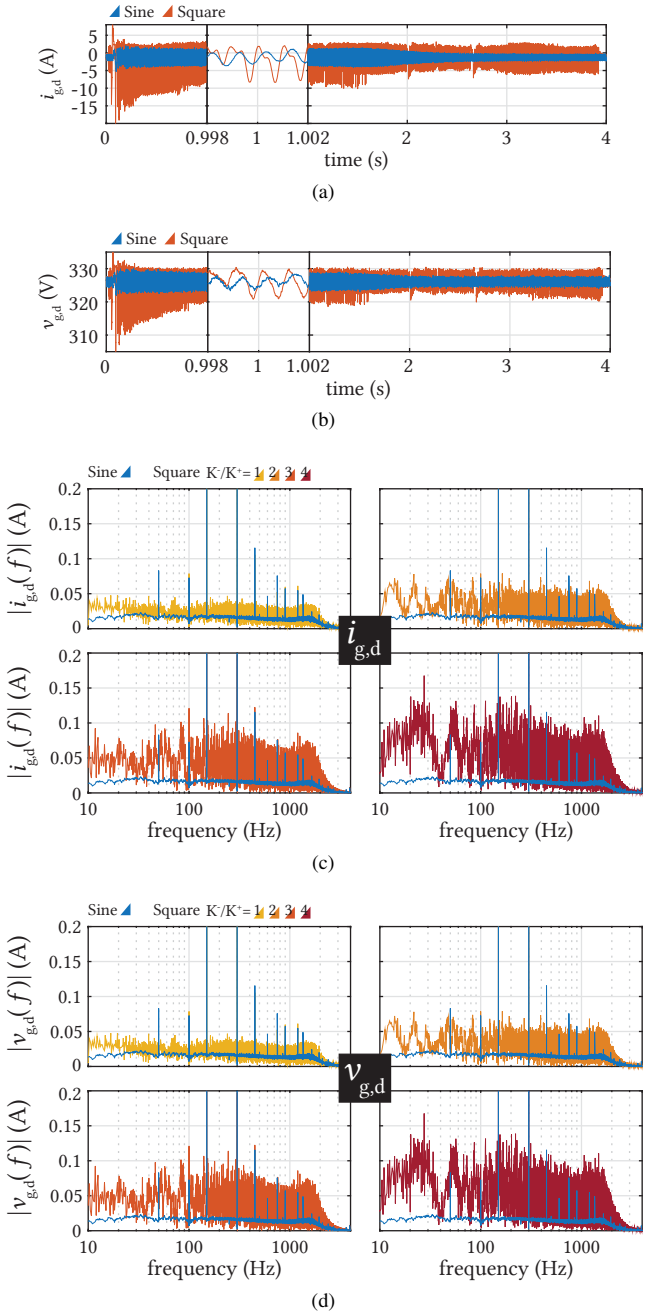

Fig. 11: Grid voltages and currents during wide-bandwidth chirp perturbation injection: $[f_{\text{chirp,beg}}, f_{\text{chirp,end}}] = [0\,\text{Hz}, 4000\,\text{Hz}]$ ($K^+ = 10\,\text{V}$, $T_{\text{FFT}} = 4\,\text{s}$, $T_{\text{injection}} = 3.9\,\text{s}$, $T_{\text{relaxation}} = 0.1\,\text{s}$), (a) currents and (b) voltages during the perturbation and (c), (d) their respective frequency decomposition.

V. Conclusion

Converter operating with a high modulation index is an issue for a converter that performs perturbation injection, as the perturbation magnitude is limited by the voltage reserve value. In this paper, a simple and easy to implement solution has been proposed to utilize the maximum of this voltage reserve. The solution is based on an asymmetric square signal enabling for higher perturbation magnitude. This asymmetry, difference between the maximum and minimum points of the signals, can be tuned as desired, with the ratio determining the signal amplitude and the frequency content of the signal. As demonstrated experimentally, the asymmetric square chirp signal has a perturbation of a frequency magnitude content much higher on average than the symmetric sine chirp signal. For wide-bandwidth signals, the signal frequency magnitude density is also much more spread along the frequency range. This method, validated experimentally, results in a better grid impedance estimation. This is hence a promising solution to address the problem of perturbation injection using grid-connected converter with limited voltage reserve.

Acknowledgment

The results presented in this paper are a part of the HYPER-RIDE project that has received funding under the European Union's Horizon 2020 research and innovation programme (Grant agreement No. 957788).

References

[1] E. Mollerstedt and B. Bernhardsson, "Out of control because of harmonics-an analysis of the harmonic response of an inverter locomotive," *IEEE Control Systems Magazine*, vol. 20, no. 4, pp. 70–81, Aug. 2000.

[2] H. Saad, Y. Fillion, S. Deschanvres, Y. Vernay, and S. Dennetière, "On Resonances and Harmonics in HVDC-MMC Station Connected to AC Grid," *IEEE Transactions on Power Delivery*, vol. 32, no. 3, pp. 1565–1573, Jun. 2017.

[3] L. Asiminoaei, R. Teodorescu, F. Blaabjerg, and U. Borup, "A digital controlled PV-inverter with grid impedance estimation for ENS detection," *IEEE Transactions on Power Electronics*, vol. 20, no. 6, pp. 1480–1490, Nov. 2005.

[4] A. Knop and F. W. Fuchs, "High frequency grid impedance analysis by current injection," in *2009 35th Annual Conference of IEEE Industrial Electronics*, Nov. 2009, pp. 536–541.

[5] T. Roinila, M. Vilkko, and J. Sun, "Online Grid Impedance Measurement Using Discrete-Interval Binary Sequence Injection," *IEEE Journal of Emerging and Selected Topics in Power Electronics*, vol. 2, no. 4, pp. 985–993, Dec. 2014.

[6] A. Riccobono, M. Mirz, and A. Monti, "Noninvasive Online Parametric Identification of Three-Phase AC Power Impedances to Assess the Stability of Grid-Tied Power Electronic Inverters in LV Networks," *IEEE Journal of Emerging and Selected Topics in Power Electronics*, vol. 6, no. 2, pp. 629–647, Jun. 2018.

[7] M. Ciobotaru, R. Teodorescu, and F. Blaabjerg, "On-line grid impedance estimation based on harmonic injection for grid-connected PV inverter," in *2007 IEEE International Symposium on Industrial Electronics*, Jun. 2007, pp. 2437–2442.

[8] M. Céspedes and J. Sun, "Online grid impedance identification for adaptive control of grid-connected inverters," in *2012 IEEE Energy Conversion Congress and Exposition (ECCE)*, Sep. 2012, pp. 914–921.

[9] A. Ghanem, M. Rashed, M. Sumner, M. A. Elsayes, and I. I. Mansy, "Grid impedance estimation for islanding detection and adaptive control of converters," *IET Power Electronics*, vol. 10, no. 11, pp. 1279–1288, 2017.

[10] Z. Ling, J. Xu, Y. Wu, Y. Hu, and S. Xie, "Adaptive Tuning of Phase-Locked Loop Parameters for Grid-Connected Inverters in Weak Grid Cases," in *2021 IEEE 16th Conference on Industrial Electronics and Applications (ICIEA)*, Aug. 2021, pp. 821–826.

[11] D. Crevier and A. Mercier, "Estimation of Higher Frequency Network Equivalent Impedances by Harmonic Analysis Natural Waveforms," *IEEE Transactions on Power Apparatus and Systems*, vol. PAS-97, no. 2, pp. 424–431, Mar. 1978.

[12] A. Robert, T. Deflandre, E. Gunther, R. Bergeron, A. Emanuel, A. Ferrante, G. Finlay, R. Gretsch, A. Guarini, J. Gutierrez Iglesias, D. Hartmann, M. Lahtinen, R. Marshall, K. Oonishi, C. Pincella, S. Poulsen, P. Ribeiro, M. Samotyj, K. Sand, J. Smid, P. Wright, and Y. Zhelesko, "Guide for assessing the network harmonic impedance," in *14th International Conference and Exhibition on Electricity Distribution. Part 1. Contributions (IEE Conf. Publ. No. 438)*, vol. 2, Jun. 1997, pp. 3/1–310 vol.2.

[13] D. Martin, E. Santi, and A. Barkley, "Wide bandwidth system identification of AC system impedances by applying pertubations to an existing converter," in *2011 IEEE Energy Conversion Congress and Exposition*, Sep. 2011, pp. 2549–2556.

[14] Z. Shen, M. Jaksic, P. Mattavelli, D. Boroyevich, J. Verhulst, and M. Belkhayat, "Three-phase AC system impedance measurement unit (IMU) using chirp signal injection," in *2013 Twenty-Eighth Annual IEEE Applied Power Electronics Conference and Exposition (APEC)*, Mar. 2013, pp. 2666–2673.

[15] Z. Liu, J. Liu, and Z. Liu, "Analysis, Design, and Implementation of Impulse-Injection-Based Online Grid Impedance Identification With Grid-Tied Converters," *IEEE Transactions on Power Electronics*, vol. 35, no. 12, pp. 12 959–12 976, Dec. 2020.

[16] G. Francis, R. Burgos, D. Boroyevich, F. Wang, and K. Karimi, "An algorithm and implementation system for measuring impedance in the D-Q domain," in *2011 IEEE Energy Conversion Congress and Exposition*, Sep. 2011, pp. 3221–3228.

[17] Z. Shen, M. Jaksic, B. Zhou, P. Mattavelli, D. Boroyevich, J. Verhulst, and M. Belkhayat, "Analysis of Phase Locked Loop (PLL) influence on DQ impedance measurement in three-phase AC systems," in *2013 Twenty-Eighth Annual IEEE Applied Power Electronics Conference and Exposition (APEC)*, Mar. 2013, pp. 939–945.

[18] M. Jaksic, Z. Shen, I. Cvetkovic, D. Boroyevich, R. Burgos, and P. Mattavelli, "Wide-bandwidth Identification of small-signal dq impedances of ac power systems via single-phase series voltage injection," in *2015 17th European Conference on Power Electronics and Applications (EPE'15 ECCE-Europe)*, Sep. 2015, pp. 1–10.